Biosensors and Bioelectronics 131 (2019) 163–170

Contents lists available at ScienceDirect

Biosensors and Bioelectronics

journal homepage: www.elsevier.com/locate/bios

Photoelectrochemical immunosensor for N^6-methyladenine detection based on Ru@UiO-66, Bi_2O_3 and Black TiO_2

Yue Wang[a], Huanshun Yin[a,*], Xuhong Li[a], Geoffrey I.N. Waterhouse[a,b], Shiyun Ai[a]

[a] College of Chemistry and Material Science, Shandong Agricultural University, Taian 271018, PR China
[b] School of Chemical Sciences, University of Auckland, Auckland 1142, New Zealand

ARTICLE INFO

Keywords:
Photoelectrochemical immunosensor
Black TiO_2
Bi_2O_3
Metal organic framework material
N^6-methyladenosine

ABSTRACT

A novel photoelectrochemical (PEC) immunosensor was successfully constructed for N^6-methyladenine (m^6A) detection based on the photoactive materials of black titanium dioxide (B-TiO_2) and bismuth trioxide (Bi_2O_3) and the signal amplification unit of $[Ru(bpy)_3]^{2+}$-doped metal organic framework (MOF). The Bi_2O_3/B-TiO_2/ITO electrode was first fabricated, then decorated with gold nanoparticles (AuNPs) which provided sites for anchoring m^6A antibodies. After the capture of m^6A via immunoreaction with the antibody, the Zr-based metal organic framework (UiO-66)-$[Ru(bpy)_3]^{2+}$ compound was further attached specifically to the phosphate group of m^6A. With visible light irradiation, a large and stable photocurrent response was produced in the presence of ascorbic acid (AA). Under optimized experimental conditions, the linear range of the PEC biosensor was 0.05–30 nM, with a low detection limit of 0.0167 nM (S/N = 3). This method showed high specificity, selectivity, stabilization and repeatability. Moreover, it was successfully used for the detection of m^6A in rice seedling leaves that had been subjected to heavy metal treatment during their development.

1. Introduction

N^6-methyladenosine (m^6A) is an important mRNA modification in mammals, insects, plants and yeasts (Narayan et al., 1994), which can affect mRNA transcription, splicing, translation and gene regulation (Wu et al., 2016). M^6A is believed to play a key role in various physiological processes, including development, fertility, cancer and a host of other human diseases (Jia et al., 2013). Though various functions have been attributed to m^6A, many functions for m^6A need to be further discovered. One of the challenges in studying m^6A is that it is typically found with low levels in mRNA samples, thereby requiring the development of reliable, sensitive and highly specific detection methods for m^6A. Existing detection methods for m^6A include high performance liquid chromatography (HPLC) (Li et al., 2017), methylated RNA immunoprecipitation followed by sequencing (MeRIP-Seq) (Meng et al., 2014), electrochemiluminescence (Lin et al., 2010), and electrochemistry (Yin et al., 2015). Although these methods can successfully detect m^6A, there are some disadvantages such as low sensitivity, complicated instrument operation and expensive and bulky instruments. As a kind of new detection technique, photoelectrochemical (PEC) assays attract special attentions since they present numerous advantages including simple operation, low cost and high sensitivity (Ge et al., 2016; Wang et al., 2018a). To date, PEC methods have been successfully applied to detect various biomolecules, including DNA, RNA and proteins, as well as small organic molecules and metal ions (Hou et al., 2018; Mei et al., 2018; Zhou et al., 2019). PEC detection technology has also been successfully used to detect m^6A. For example, Wang et al. used Ag^+-mediated cytosine pairs for signal amplification to detect m^6ATP (Wang et al., 2018a). Although this method offered good specificity and sensitivity, the assay was not ideal since it took a long time. Accordingly, the development of novel PEC detection strategies for m^6A with short detection times is an urgent research priority.

In order to achieve high detection sensitivity, photoactive materials with high photoelectric conversion efficiencies are critical for PEC biosensor fabrication. Commonly used photoactive materials are TiO_2 (Tang et al., 2011), g-C_3N_4 (Da et al., 2018), CdS (Hou et al., 2016), Bi_2S_3 (Cui et al., 2018), WS_2 (Zhou et al., 2018, 2019), etc. Among them, TiO_2 is the widely most studied semiconductor due to its low-cost, non-toxicity, high chemical durability and excellent photocatalytic efficiency under UV irradiation (Shen et al., 2017). However, pristine TiO_2 is not conducive to generate PEC signal under visible light because of its wide band gap (3.2 eV) (Chakraborty et al., 2014). This limits the application of traditional TiO_2 materials in PEC biosensor fabrication. Recent studies have reported that the hydrogenation of white TiO_2 by reaction with $NaBH_4$ at 300–350 °C produces black titanium dioxide (B-TiO_2). The B-TiO_2 product contains an abundance of oxygen vacancies

* Corresponding author.
E-mail address: yinhs@sdau.edu.cn (H. Yin).

https://doi.org/10.1016/j.bios.2019.01.064
Received 6 December 2018; Received in revised form 23 January 2019; Accepted 31 January 2019
Available online 18 February 2019
0956-5663/

(effectively TiO_{2-x}), resulting in full absorption across the visible spectrum and the increased visible light-driven photocatalytic activity (Chen et al., 2015). The band gap of B-TiO_2 is significantly narrowed (E_g = 1.85 eV), thereby affording a stronger photocurrent response under visible light (Ullattil et al., 2018). Accordingly, B-TiO_2 maybe a very promising photoactive material for PEC biosensor fabrication, which can motivating a detailed investigation of its application potential. Bismuth oxide (Bi_2O_3) is an important conductive material with a narrow band gap (E_g = 2.8 eV) (Jiang et al., 2018). However, due to the rapid recombination of photocurrent carriers, its efficiency under visible light needs to be improved. Bi_2O_3 is a *p*-type semiconductor and TiO_2 is an *n*-type semiconductor. Thus, Bi_2O_3 and TiO_2 can be coupled to form a *p-n* heterojunction (Huang et al., 2017). The formation of heterojunction of Bi_2O_3/B-TiO_2 can improve the separation efficiency of photoexcited electron-hole pair and greatly increase the intensity of photocurrent. B-TiO_2/Bi_2O_3 heterojunction also has great application potential in the construction of biosensors. Metal-organic frameworks (MOFs) are 3-dimensional coordination polymers, which composes of metal cations or metal clusters bridged together by organic linkers. They possess high specific surface areas, well-defined pore architectures and strong light collection abilities (Wang et al., 2015). Currently, MOFs are attracting tremendous research interest in many fields, such in adsorption, gas storage, catalysis and drug delivery (Cao et al., 2018; Jabbari et al., 2016; Zhang et al., 2018), especially in biosensor fabrication. The MOF UiO-66, constructed from $[Zr_6O_4(OH)_4]$ clusters with 1,4-benzenedicarboxylate struts, is chemically stable, non-toxic with good biocompatibility, and has a high porosity that allows accommodation of various photosensitive molecules. Therefore, it could be potentially exploited in PEC biosensor development as a means of improving the light harvesting efficiency and photoelectric conversion efficiency (Wang et al., 2017; Yan et al., 2018). Some oxides are known to have a strong affinity for phosphate groups, such as ZrO_2, TiO_2, Al_2O_3, ZnO and Fe_2O_3 (Bai et al., 2013; Miao et al., 2012). Accordingly, the $[Zr_6O_4(OH)_4]$ clusters in UiO-66 are also expected to possess the ability to strongly bind with phosphate groups, making UiO-66 a promising material for constructing biosensors for mRNA and DNA since these biomolecules have abundant phosphate groups.

In this experiment, a new PEC biosensor was constructed for detecting N^6-methyladenosine-5′-triphosphate (m^6ATP) using B-TiO_2, Bi_2O_3 and Ru@UiO-66 as photoactive materials. In order to obtain a strong photoelectric signal, a novel Bi_2O_3/B-TiO_2/ITO was employed as substrate electrode. The specificity of detection was achieved through the specific interaction between m^6ATP and its antibody (anti-m^6A). Finally, Ru@UiO-66 identified the phosphate groups of m^6ATP with the amplified signal by the $[Ru(bpy)_3]^{2+}$ complex (Yan et al., 2018). The developed PEC immunosensor strategy offers a easy and fast way for the detection of m^6ATP.

2. Experimental

2.1. Chemicals and reagents

N^6-methyladenosine-5′-triphosphate (m^6ATP) was obtained from TriLink BioTechnologies, Inc. (San Diego, USA). Anti-N^6-methyladenosine (m^6A) antibody was purchased from Abcam (USA). The detailed chemicals and reagents are displayed in Supporting information.

2.2. Instruments

Electrochemical impedance spectroscopy (EIS) measurements were performed on a CHI660C electrochemical workstation (CH instruments, Austin, USA). PEC measurements were performed on a home-built PEC system equipped a three-electrode system. The detailed instruments are displayed in Supporting information.

2.3. Synthesis of AuNPs, B-TiO_2 and Ru@UiO-66

Gold nanoparticles (AuNPs) were prepared according to a literature method (Wang et al., 2018b). Briefly, 96 mL of ultrapure water and 4 mL $HAuCl_4$ (0.05 M) were added to a two-neck flask (The final $HAuCl_4$ concentration was 2 mM). When the solution began to reflux, 20 mL sodium citrate solution (38.8 mM) was added into the flask. The solution color turned dark red within 1 min. The dispersion was then refluxed for 20 min and then naturally cooled. The acquired AuNPs solution was deposited at 4 °C until use.

B-TiO_2 was synthesized according to a reported method (Naldoni et al., 2012). TiO_2 (1 g) and $NaBH_4$ (1 g) were mixed together by grinding with a mortar and pestle for 15 min. Next, the uniformly mixed powder was spread evenly on the bottom of the porcelain boat, after which the porcelain boat was transferred to a tube furnace and heated to 300 °C at 5 °C/min under a nitrogen atmosphere. The temperature was maintained at 300 °C for 30 min, after which the sample was cooled to room temperature at 5 °C/min. The product was washed repeatedly with deionized water to remove any unreacted $NaBH_4$ or side products. Finally, the B-TiO_2 product was dried under vacuum at 60 °C.

UiO-66 was prepared according to a previous paper with some modification (Wang et al., 2015). Briefly, 0.48 g of zirconium chloride, 8 mL of CH_3COOH and 0.236 mL of H_2O were fully dissolved in 64 mL of diethylpyrocarbonate. Then 189.88 mg 1,4-benzenedicarboxylic acid was evenly dispersed in the solution. Subsequently, the homogeneous solution was transferred to a 100 mL Teflon-lined autoclave. The autoclave was maintained at 120 °C for 24 h. After cooling, the collected UiO-66 crystals were washed three times with N,N-dimethylformamide. Finally, the white UiO-66 crystals were soaked in methanol for three days to remove any residual DMF. The obtained crystals were dried at 60 °C for 6 h under vacuum. The UiO-66 powder was produced by lightly grinding the product with a mortar and pestle. To prepare Ru@UiO-66, 2 mg of UiO-66 and 6 mg of $[Ru(bpy)_3]Cl_2{\cdot}6H_2O$ were added to 10 mL ultrapure water, and the resulting dispersion was stirred at 25 °C for 36 h. The Ru@UiO-66 product was collected by centrifugation and dried for further use.

2.4. Immunosensor fabrication and PEC measurement

Firstly, the ITO glass was cut into pieces with the size of 5 × 1 cm^2. Then, these ITO pieces were pretreated according to literature method (Wang et al., 2018b). Subsequently, 40 μL B-TiO_2 dispersion (6 mg/mL in water) was dropped onto the ITO conductive glass piece and dried under an infrared lamp (the obtained electrode is denoted as B-TiO_2/ITO). Next, 40 μL of Bi_2O_3 dispersion (5 mg/mL) and 40 μL of the AuNPs suspension were dropped successively onto the B-TiO_2/ITO electrode surface (in each case the addition of the nanomaterial was followed by a drying step under the infrared lamp). The fabricated electrodes were denoted as Bi_2O_3/B-TiO_2/ITO and AuNPs/Bi_2O_3/B-TiO_2/ITO, respectively. The AuNPs/Bi_2O_3/B-TiO_2/ITO electrode was incubated with 20 μL MPBA (0.1 mM) for 30 min at 37 °C in a humid cell (the electrode is denoted as MPBA/AuNPs/Bi_2O_3/B-TiO_2/ITO), followed by rinsing with deionized water for three times. Subsequently, 20 μL of 5 μg/mL m^6A antibody solution was dropped onto the MPBA/AuNPs/Bi_2O_3/B-TiO_2/ITO electrode surface, which was then incubated at 37 °C for one hour in a humidified chamber. The electrode surface was then rinsed with the washing buffer for three times (yielding Ab/MPBA/AuNPs/Bi_2O_3/B-TiO_2/ITO). Next, the electrode was incubated with 20 μL of different concentrations of m^6ATP at 37 °C for one hour in a wettish environment. The prepared electrode (m^6ATP/Ab/MPBA/AuNPs/Bi_2O_3/B-TiO_2/ITO) was washed thoroughly with washing buffer for three times. Finally, 40 μL of 4 mg/mL Ru@UiO-66 dispersion was dropped onto the electrode surface and the resulting electrode (Ru/m^6ATP/Ab/MPBA/AuNPs/Bi_2O_3/B-TiO_2/ITO) was incubated for one hour at room temperature.

PEC detection was carried out at room temperature in 0.01 M PBS

containing 0.01 M AA (pH 7.4) solution. During the photocurrent measurements, AA was employed as a sacrificial electron donor. And the photocurrent was measured by the custom-built PEC workstation under visible light and the applied potential of − 0.3 V.

2.5. Sample preparation

Mature rice seeds were purchased from a local market in Taian, China. The rice seeds were immobilized in gauze, placed in a petri dish and then immersed in deionized water for one week at 25 °C to achieve germination. $Pb(NO_3)_2$ solutions with a concentration of 1, 10, 20, 50, 100 mg/L (each 200 mL) were prepared, and used to culture the leaves of five groups of rice seedlings for 24 h. A group of rice seedlings was also cultured with water, which was used as control.

Extraction of total RNA: Firstly, 0.1 g of the leaves of the rice seedlings were harvested and transferred to a mortar. After that, 1 mL of Trizol was added and the leaves were ground into a slurry under liquid nitrogen. Next, the slurry and 0.2 mL of $CHCl_3$ were added into a 1.5 mL centrifuge tube and shaken at room temperature for 5 min. Then, it was centrifuged at 12,000 rpm for 15 min at 4 °C. The supernatant was collected, and then 0.5 mL of isopropanol was added into the supernatant. The tube was then placed at room temperature for 10 min, followed by centrifugation at 12,000 rpm for 10 min at 4 °C. Subsequently, the supernatant was discarded and 1 mL of DEPC sterilized water was added to the solid residue. Following centrifugation, the supernatant was discarded and 200 μL of DEPC sterilized water added to the sediment. Finally, the total RNA was collected after centrifugation and dispersed in 10 mM Tris-HCl (pH 7.4). The total RNA concentration was measured with a Quawell Q5000 micro volume spectrophotometer (USA). To obtain the oligonucleotides containing m^6ATP, the total RNA was diluted to a constant concentration, and then the solution was treated with 0.1 mg/mL RNase A for 2 h at 37 °C. Finally, the RNA was put in a freezer and stored at − 80 °C.

3. Results and discussion

3.1. Detection strategy of PEC immunosensor

Scheme 1 shows the fabrication procedure of the PEC immunosensor for m^6ATP detection. Firstly, B-TiO_2 and Bi_2O_3 are successively deposited on the ITO electrode to provide a good photoelectric platform. Subsequently, AuNPs are further modified on Bi_2O_3/B-TiO_2/ITO surface by physical adsorption. Then, MPBA is captured on electrode surface via Au-S bond formation. Based on the covalent reaction between boric acid group of MPBA and the glycosyl group in the m^6A antibody, the modification of antibody on electrode surface is achieved. Next, the m^6ATP target is further captured by its specific immunoreaction with the m^6A antibody, resulting in the phosphate group of m^6ATP being oriented away from the electrode surface. Subsequently, Ru@UiO-66 is captured by interactions between the Zr-O clusters in MOF and the phosphate groups of m^6ATP. The $[Ru(bpy)_3]^{2+}$ contained within Ru@UiO-66 can then be used for signal amplification via absorption of visible light and the generation of excited electrons. Injected of the excited electrons into the conduction band of B-TiO_2 produces Ru^{3+}. Addition of ascorbic acid (AA) as a sacrificial electron donor converts any Ru^{3+} to form back to Ru^{2+}, thereby delivering a consecutive photocurrent. By this strategy, the magnitude of the photocurrent is connected with the concentration of m^6ATP, thereby allowing the detection and quantification of m^6ATP.

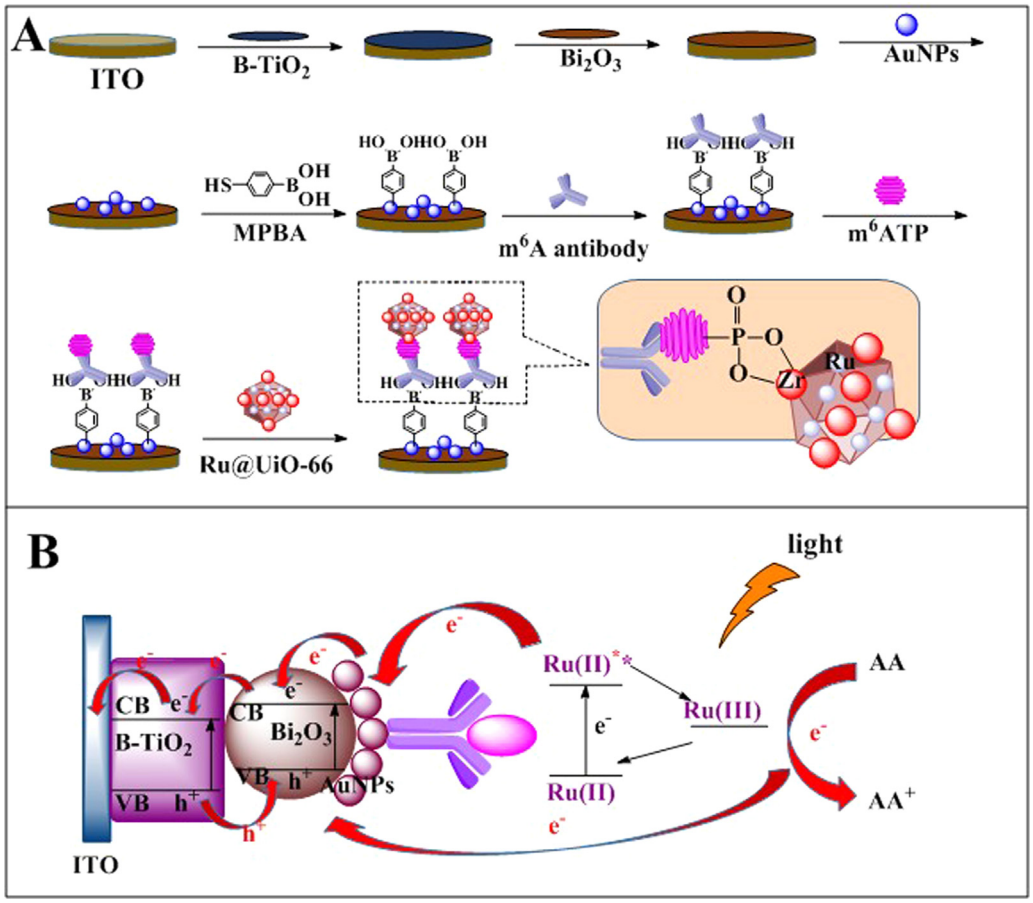

Scheme 1. (A) Schematic illustration of the fabrication procedure of the PEC immunosensor. (B) Mechanism of photocurrent generation of the PEC immunosensor.

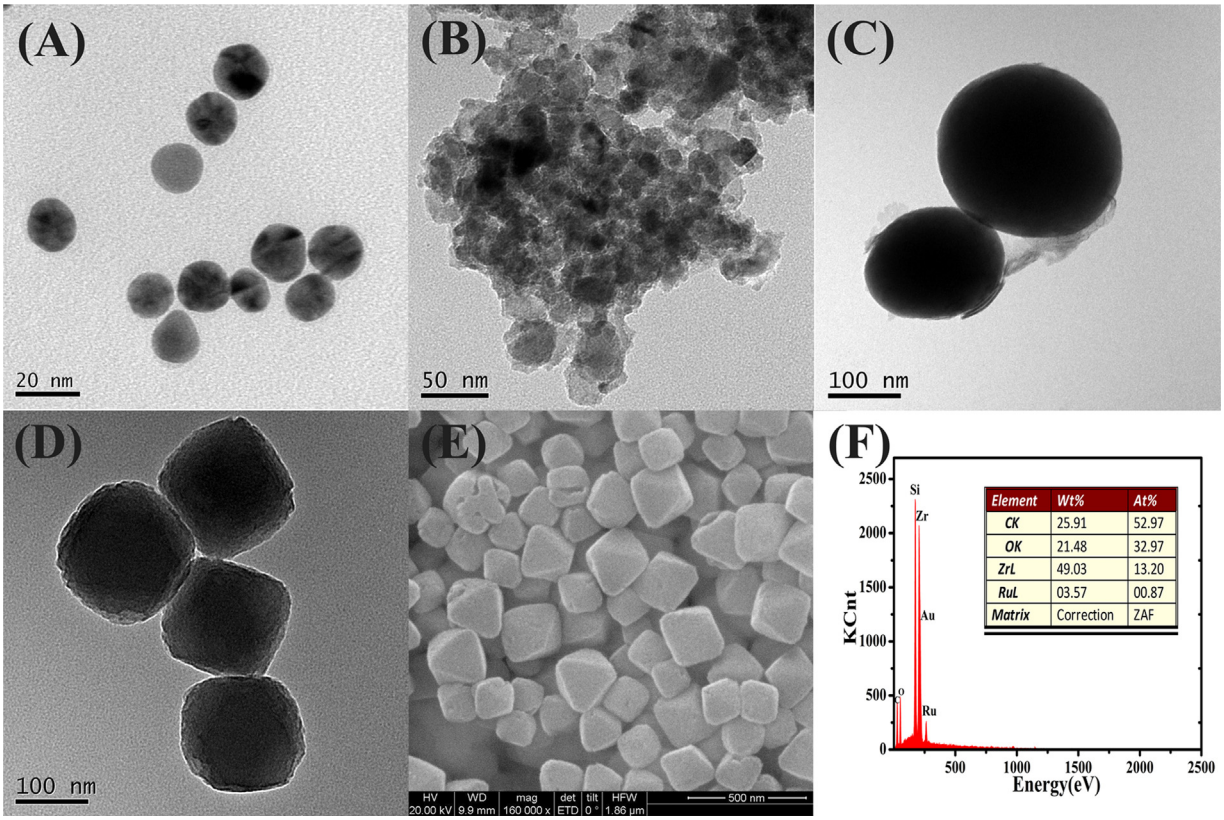

Fig. 1. TEM images of AuNPs (A), B-TiO_2 (B), Bi_2O_3 (C) and UiO-66 (D). SEM image of Ru@UiO-66 (E). EDS spectrum of Ru@UiO-66 (F).

3.2. Characterization of AuNPs, B-TiO_2, Bi_2O_3, UiO-66 and Ru@UiO-66

TEM was used to examine the size and morphologies of the AuNPs, B-TiO_2, Bi_2O_3 and UiO-66 materials. The AuNPs were quasi-spherical particles with an average diameter around 15 nm (Fig. 1A). The B-TiO_2 nanoparticles had an individual diameter less than 50 nm, but existed in the form of aggregates (Fig. 1B). The Bi_2O_3 particles were ovoid with diameters in the range 100–300 nm (Fig. 1C). UiO-66 possessed with a cubic morphology, as revealed by TEM (Fig. 1D) and the SEM image of Ru@UiO-66 (Fig. 1E). The EDS spectrum of Ru@UiO-66 (Fig. 1F) confirms the presence of C, O, Zr and Ru. The signal for N in the dipyridyl ligands is obscured by the intense signals of C and O. The EDS data, in particular the identification of Ru, confirms the successfully synthesis of Ru@UiO-66 particles.

3.3. EIS characterization

Electrochemical impedance spectroscopy (EIS) is an efficient method for probing the interfacial characteristics of electrodes, which is invaluable for monitoring the success of individual steps in the fabrication of biosensors. The bare ITO electrode has an interface electron transfer resistance (R_{et}) of about 120 Ω (Fig. 2, curve a). After deposition of B-TiO_2 (curve b) and Bi_2O_3 (curve c) on the surface of the ITO electrode, the R_{et} value increases. It can be ascribed to the immobilized semiconductor nanomaterials, which block the diffusion of the redox probe to electrode surface (resulting in an increased interface electron transfer resistance). After AuNPs are deposited on the modified electrode surface (curve d), the R_{et} value decreases due to the high electrical conductivity of the AuNPs, which motivated the electron transfer. However, after MPBA (curve e) attaches to the AuNPs, R_{et} value increases due to repulsion between the negatively charged groups of MPBA and the negatively charged $Fe(CN)_6^{3-/4-}$ probe. As expected, the R_{et} values increases when m^6A antibodies (curve f) and m^6ATP (curve g) attach to the electrode surface. It can be attributed to the large volume of the antibody and m^6ATP (i.e. steric effects) and also the negatively charges phosphate group on m^6ATP (i.e. electrostatic effects), which act collectively to hinder the diffusion of the redox probe. Similarly, attachments of bulky Ru@UiO-66 causes a further increase in the R_{et} value (curve h), which is again attributed to steric-hindrance effect. The data in Fig. 2 thus illustrates that each step in the biosensor fabrication process was successful, whilst also illustrating the merits of EIS for tracking each stage of biosensor fabrication.

3.4. Detection feasibility

The detection feasibility of the developed method for m^6ATP detection was investigated by comparing the PEC response of different modified electrodes in the detection buffer. As showed in Fig. 2B, the PEC responses for B-TiO_2/ITO (curve b) and Bi_2O_3/ITO (curve a) are 440 and 140 nA, respectively. These results demonstrate that both B-TiO_2 and Bi_2O_3 possess good photoactivity. However, the photocurrent increases greatly to 965 nA for the Bi_2O_3/B-TiO_2/ITO electrode, indicating that Bi_2O_3 can effectively enhance the photocurrent response of B-TiO_2. It can be ascribed to the formation of a Bi_2O_3/B-TiO_2 heterojunction. Under the irradiation of visible light, the transfer of electrons from the conduction band (CB) of Bi_2O_3 to the CB of B-TiO_2 (with holes created by photo-excitation in the VB of B-TiO_2 migrating across the heterojunction to the VB of Bi_2O_3). The heterojunction thus increases the availability of charge carriers by suppressing the recombination of photoelectrons and holes (Bian et al., 2008), thereby affording a high photocurrent. Accordingly, Bi_2O_3/B-TiO_2/ITO was used in this work as the photoactive substrate for immobilizing the biomolecules in PEC biosensor development.

Fig. 2C shows the feasibility analysis on the biosensor. The bare ITO electrode (curve a) shows no photocurrent response in 0.01 M PBS containing 0.01 M AA under visible light irradiation. The Bi_2O_3/B-TiO_2/ITO (curve b) electrode illustrates a strong photocurrent response, indicating that the semiconducting materials have been successfully

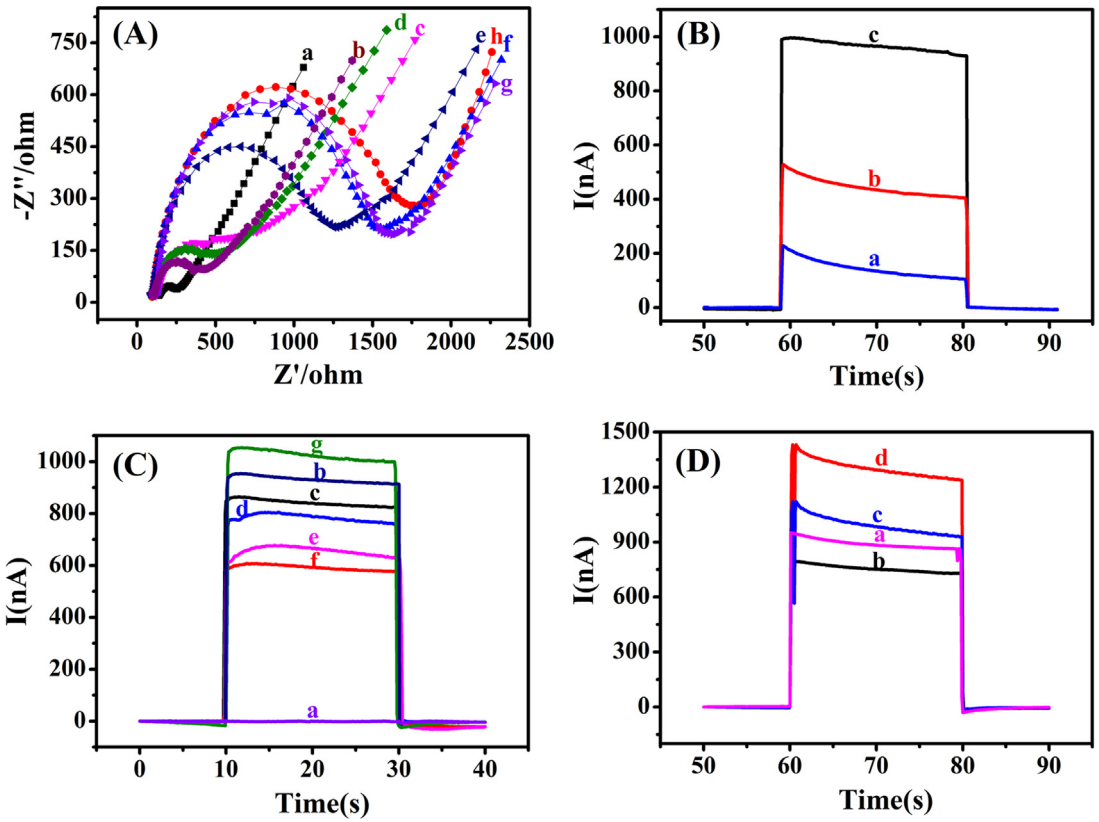

Fig. 2. (A) Nyquist diagrams showing EIS data for different electrodes recorded from 0.01 Hz to 10^5 Hz in 10 mM Tris-HCl containing 5 mM $[Fe(CN)_6]^{3-/4-}$ (1:1) and 10 mM KCl (pH 7.4). (a) ITO, (b) B-TiO_2/ITO, (c) Bi_2O_3/B-TiO_2/ITO, (d) AuNPs/Bi_2O_3/B-TiO_2/ITO, (e) MPBA/AuNPs/Bi_2O_3/B-TiO_2/ITO, (f) Ab/MPBA/AuNPs/Bi_2O_3/B-TiO_2/ITO, (g) m^6ATP/Ab/MPBA/AuNPs/Bi_2O_3/B-TiO_2/ITO, (h) Ru/m^6ATP/Ab/MPBA/AuNPs/Bi_2O_3/B-TiO_2/ITO. (B) The photocurrent of (a) Bi_2O_3/ITO, (b) B-TiO_2/ITO and (c) Bi_2O_3/B-TiO_2/ITO in 0.01 M PBS (pH 7.4) containing 0.01 M AA. (C) The photocurrent response of different electrodes in 0.01 M PBS containing 0.01 M AA. (a) ITO, (b) Bi_2O_3/B-TiO_2/ITO, (c) AuNPs/Bi_2O_3/B-TiO_2/ITO, (d) MPBA/AuNPs/Bi_2O_3/B-TiO_2/ITO, (e) Ab/MPBA/AuNPs/Bi_2O_3/B-TiO_2/ITO, (f) m^6ATP/Ab/MPBA/AuNPs/Bi_2O_3/B-TiO_2/ITO, (g) Ru/m^6ATP/Ab/MPBA/AuNPs/Bi_2O_3/B-TiO_2/ITO (D) The photocurrent response in 0.01 M PBS (pH 7.4) containing 0.01 M AA of different photoelectrodes. (a) Bi_2O_3/B-TiO_2/ITO, (b) UiO-66/Bi_2O_3/B-TiO_2/ITO, (c) Ru/Bi_2O_3/B-TiO_2/ITO, (d) Ru@UiO-66/Bi_2O_3/B-TiO_2/ITO.

deposited on the ITO electrode. After AuNPs are deposited on the Bi_2O_3/B-TiO_2/ITO electrode (curve c), the photocurrent response decreases. This decrease is explained by vibration relaxation associated with the localized surface plasmon resonance of the AuNPs under visible light irradiation (also absorption of light by the AuNPs might reduce the amount of light reaching the underlying photoactive layer). It is well known that AuNPs can react with –SH to form Au-S bond. Thus, in this work, AuNPs are employed as the immobilization matrix of MPBA. As shown in curve d, the photocurrent response decreases when MPBA is modified on electrode surface, which can be ascribed to the fact that MPBA hinders the transfer of electron donors. Subsequently, when antibodies (curve e) and then m^6ATP (curve f) are captured on the MPBA/AuNPs/Bi_2O_3/B-TiO_2/ITO electrode, the photocurrent decreases in successive increments. The antibodies and m^6ATP may inhibit AA diffusion to the electrode surface where it reacts with the photogenerated holes, thereby reducing the photocurrent. Finally, after the modification with Ru@UiO-66 (curve g), the photocurrent response increases significantly, proving conclusively that Ru@UiO-66 has a signal amplification effect. The PEC results confirmed that each electrode modification step was successful.

To further prove the signal amplification effect of Ru@UiO-66, several additional PEC experiments were carried out in detection buffer. Fig. 2D (curve a) shows the PEC response of Bi_2O_3/B-TiO_2/ITO (880 nA). After modification with UiO-66, the photocurrent of UiO-66/Bi_2O_3/B-TiO_2/ITO decreases to 750 nA (curve b), indicating that UiO-66 exerts an inhibition effect on the PEC response. However, when $[Ru(bpy)_3]^{2+}$ is adsorbed on the Bi_2O_3/B-TiO_2/ITO surface, the photocurrent of the electrode increases (curve c). However, due to the limited amount of $[Ru(bpy)_3]^{2+}$ which can be immobilized in the absence of UiO-66, the photocurrent increase is small. However, the photocurrent increases greatly when UiO-66 is employed as the carrier of $[Ru(bpy)_3]^{2+}$ (curve d), and the photocurrent of Ru@UiO-66/Bi_2O_3/B-TiO_2/ITO electrode achieves to 1300 nA. The strong π-π stacking and Van Der Waals interactions between $[Ru(bpy)_3]^{2+}$ and UiO-66 facilitates the injection of electrons from $[Ru(bpy)_3]^{2+}$ into the electrode, thereby boosting the photocurrent. The data in Fig. 2D thus confirms the signal amplification effect of Ru@UiO-66.

3.5. Optimal conditions for experiment

In order to achieve a high detection sensitivity for m^6ATP using this PEC immunosensor, several experimental conditions were optimized. The optimization results are as follows (The detailed description is in Supplementary materials). B-TiO_2 concentration is 6 mg/mL, Bi_2O_3 concentration is 5 mg/mL, m^6A antibody immobilization time is 60 min, Ru@UiO-66 concentration is 4 mg/mL, and Ru@UiO-66 immobilization time is 60 min (Fig. 3).

3.6. Analytical performance of the PEC immunosensor

Under optimized experimental conditions, the PEC immunosensor was applied to evaluate the relationship between the photocurrent and the m^6ATP concentration. As shown in Fig. 4A, the photocurrent response of the immunosensor increases with increasing m^6ATP

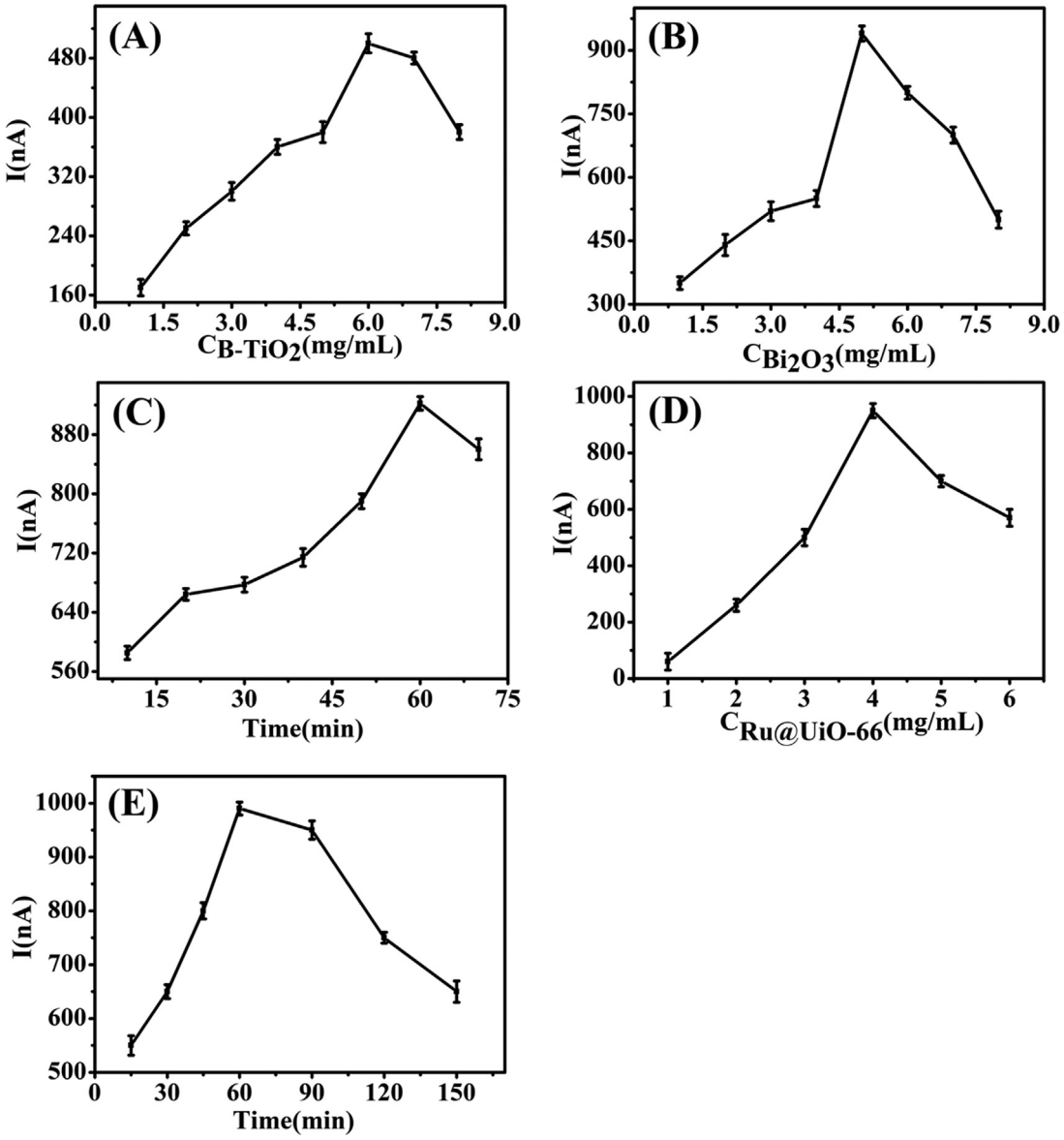

Fig. 3. Effects of B-TiO_2 concentration (A), Bi_2O_3 concentration (B), m^6A antibody immobilization time (C), Ru@UiO-66 concentration (D) and Ru@UiO-66 immobilization time (E) on the PEC response of the biosensor. The error bars represent the standard deviation of three measurements.

concentration. The photocurrent is proportional to the logarithm of the m^6ATP concentration in the range 0.05–30 nM (Fig. 4B). The linear regression equation can be expressed as I (nA) = 343.63 log$c$ (nM) + 534.45 (R = 0.9979) and the detection limit is estimated to be 0.0167 nM (S/N = 3) (Feng et al., 2018).

Detection specificity is an important parameter for PEC biosensors. In order to verify that the PEC biosensor possesses excellent detection specificity, four additional biosensors were prepared by replacing m^6ATP with AMP, CMP, GMP and UMP. The PEC response of each immunosensor was recorded. Fig. 4C shows the change of the photocurrent ($\Delta I = I_1 - I_0$), where I_1 is the measured photocurrent of different immunosensor, and I_0 is the photocurrent of the Ab/MPBA/AuNPs/Bi_2O_3/B-TiO_2/ITO electrode. The photocurrent response change for AMP, CMP, GMP, and UMP are low. However, in the presence of m^6ATP, a strong current response change is measured, confirming that the biosensor had very high selectivity for m^6ATP.

The reproducibility of the biosensor was examined by constructing seven Ru/m^6ATP/Ab/MPBA/AuNPs/Bi_2O_3/B-TiO_2/ITO electrodes in parallel. Fig. 4D shows that the photocurrent signals of the seven electrodes were very similar, with a relative standard deviation of only 1.51%, demonstrating that electrode had very good reproducibility.

3.7. Rice seedlings samples analysis

In order to test the applicability of the immunosensor for the detection of m^6A, the immunosensor was applied to the detection of m^6A in the leaves of rice seedlings that had been treated with different concentrations of $Pb(NO_3)_2$ solutions. As shown in Fig. 5, the expression level of m^6A in the leaves of rice seedlings decreases with increasing Pb $(NO_3)_2$ concentration. Results indicate that Pb^{2+} concentration effects the expression level of m^6A, thereby offering useful information about the eco-toxicological effects of Pb^{2+} on rice development.

4. Conclusion

In summary, a PEC immunoassay was developed using Bi_2O_3/B-TiO_2 nanocomposites as photoactive material and Ru@UiO-66 as the phosphate identification unit and signal amplification unit for detecting m^6A. The Bi_2O_3/B-TiO_2 heterojunction effectively improves the separation of e^-/h^+ and significantly enhances the photocurrent signal. In

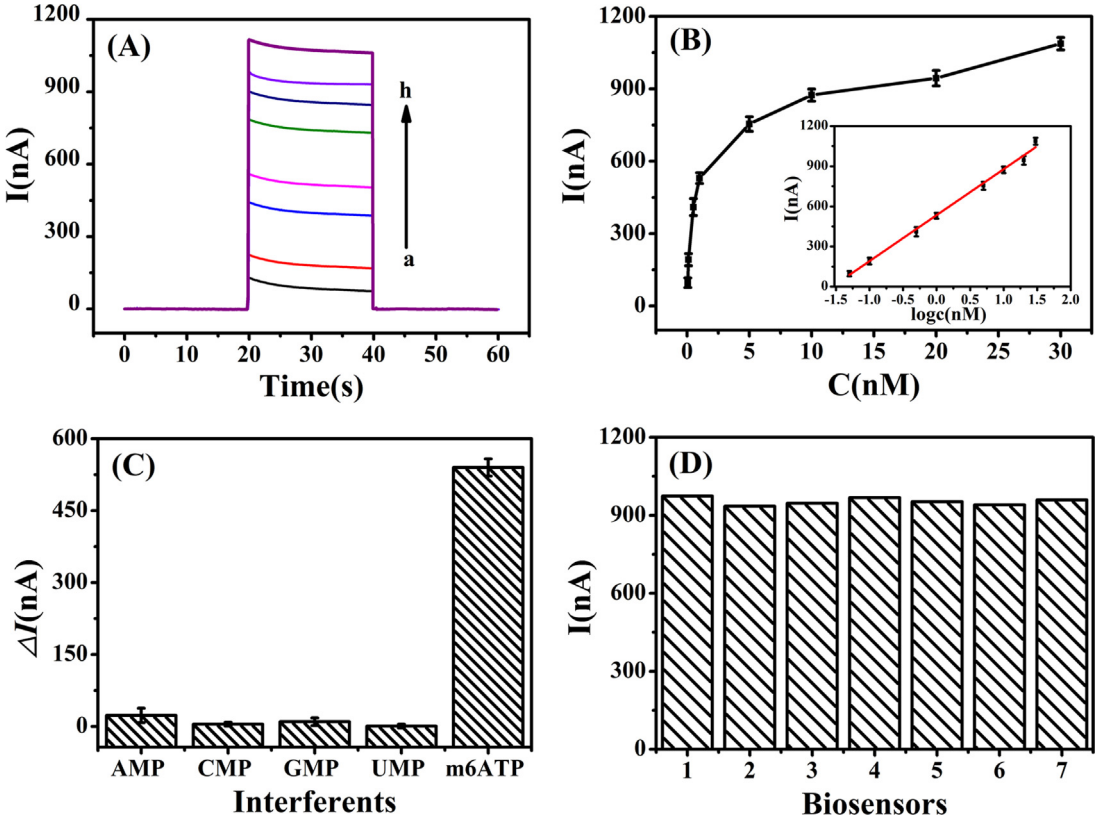

Fig. 4. (A) The PEC response of the biosensor with different concentrations of m^6ATP. a-h, 0.05, 0.1, 0.5, 1, 5, 10, 20, 30 nM, respectively. (B) The relationship between the photocurrent and m^6ATP concentration. Inset: The linear relationship between the photocurrent and the logarithm value of the m^6ATP concentration. (C) Selectivity of the immunosensor towards different targets (target concentration 10 nM). (D) The photocurrent response of seven immunosensors fabricated independently. M^6ATP concentration is 10 nM.

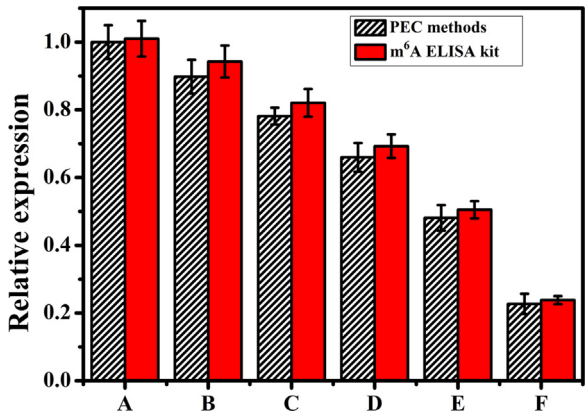

Fig. 5. Histogram of the expression level of m^6A in the leaves of rice seedlings after incubation with different concentrations of Pb^{2+}. The error bars in each plot represent the standard deviation of three measurements. A-F, 0, 1, 10, 20, 50, 100 mg/L Pb^{2+}, respectively.

addition, the high porosity of UiO-66 facilitates the enrichment of $[Ru(bpy)_3]^{2+}$, and the excited state electrons generated by $[Ru(bpy)_3]^{2+}$ under visible light irradiation can be transferred to the Bi_2O_3/B-TiO_2/ITO photoelectrode to boost the photocurrent response. The linear detection range is 0.05–30 nM and m^6ATP detection limit is 0.0167 nM. The results show that this method has good selectivity, specificity and sensitivity, and can effectively detect m^6A. Moreover, this method was successfully applied to detect m^6A in biological samples. Thus this work has great application potential in the research of m^6A biological function.

Acknowledgements

This work was supported by the National Natural Science Foundation of China (Nos. 41807484, 21775090), the Natural Science Foundation of Shandong Province, China (Nos. ZR2016BM10 and ZR2018MB028). GINW acknowledges funding support from the Ministry of Business Innovation and Employment (MBIE) Catalyst Fund, Contract MAUX1609: "Disruptive Technologies from Metal-Organic Frameworks".

Credit author statement

All the authors have been contributed for this work.

All the authors have been have made a significant contribution to the Conceptualization, Data curation, Formal analysis, Funding acquisition, Investigation, Methodology of the reported study.

Declaration of interests

None.

Appendix A. Supporting information

Supplementary data associated with this article can be found in the online version at https://doi.org/10.1016/j.bios.2019.01.064

References

Bai, J., Zhao, Y., Wang, Z., Liu, C., Wang, Y., Li, Z., 2013. Anal. Chem. 85, 4813–4821.
Bian, Z., Zhu, J., Wang, S., Cao, Y., Qian, X., Li, H., 2008. J. Phys. Chem. C 112, 6258–6262.
Cao, J., Yang, Z.-h., Xiong, W.-p., Zhou, Y.-y., Peng, Y.-r., Li, X., Zhou, C.-y., Xu, R.,

Zhang, Y.-r., 2018. Chem. Eng. J. 353, 126–137.
Chakraborty, A.K., Hossain, M.E., Rhaman, M.M., Sobahan, K.M.A., 2014. J. Environ. Sci. 26, 458–465.
Chen, X., Liu, L., Huang, F., 2015. Chem. Soc. Rev. 44, 1861–1885.
Cui, L., Hu, J., Wang, M., Diao, X.-k., Li, C.-c., Zhang, C.-y., 2018. Anal. Chem. 90, 11478–11485.
Da, H., Liu, H., Zheng, Y., Yuan, R., Chai, Y., 2018. Biosens. Bioelectron. 101, 213–218.
Feng, J., Li, F., Li, X., Wang, Y., Fan, D., Du, B., Li, Y., Wei, Q., 2018. Biosens. Bioelectron. 117, 773–780.
Ge, L., Wang, W., Hou, T., Li, F., 2016. Biosens. Bioelectron. 77, 220–226.
Hou, T., Xu, N., Wang, W., Ge, L., Li, F., 2018. Anal. Chem. 90, 9591–9597.
Hou, T., Zhang, L., Sun, X., Li, F., 2016. Biosens. Bioelectron. 75, 359–364.
Huang, Y., Wei, Y., Wang, J., Luo, D., Fan, L., Wu, J., 2017. Appl. Surf. Sci. 423, 119–130.
Jabbari, V., Veleta, J.M., Zarei-Chaleshtori, M., Gardea-Torresdey, J., Villagrán, D., 2016. Chem. Eng. J. 304, 774–783.
Jia, G., Fu, Y., He, C., 2013. Trends Genet. 29, 108–115.
Jiang, L., Yuan, X., Zeng, G., Liang, J., Chen, X., Yu, H., Wang, H., Wu, Z., Zhang, J., Xiong, T., 2018. Appl. Catal. B: Environ. 227, 376–385.
Li, Q., Li, X., Tang, H., Jiang, B., Dou, Y., Gorospe, M., Wang, W., 2017. J. Cell Biochem. 118, 2587–2598.
Lin, Z., Wang, W., Jiang, Y., Qiu, B., Chen, G., 2010. Electrochim. Acta 56, 644–648.
Mei, L.-P., Jiang, X.-Y., Yu, X.-D., Zhao, W.-W., Xu, J.-J., Chen, H.-Y., 2018. Anal. Chem. 90, 2749–2755.
Meng, J., Lu, Z., Liu, H., Zhang, L., Zhang, S., Chen, Y., Rao, M.K., Huang, Y., 2014. Methods 69, 274–281.
Miao, P., Ning, L., Li, X., Li, P., Li, G., 2012. Bioconjugate Chem. 23, 141–145.
Naldoni, A., Allieta, M., Santangelo, S., Marelli, M., Fabbri, F., Cappelli, S., Bianchi, C.L., Psaro, R., Dal Santo, V., 2012. J. Am. Chem. Soc. 134, 7600–7603.
Narayan, P., Ludwiczak, R.L., Goodwin, E.C., Rottman, F.M., 1994. Nucleic Acids Res. 22, 419–426.
Shen, L., Xing, Z., Zou, J., Li, Z., Wu, X., Zhang, Y., Zhu, Q., Yang, S., Zhou, W., 2017. Sci. Rep. 7, 41978.
Tang, J., Tang, D., Li, Q., Su, B., Qiu, B., Chen, G., 2011. Anal. Chim. Acta 697, 16–22.
Ullattil, S.G., Narendranath, S.B., Pillai, S.C., Periyat, P., 2018. Chem. Eng. J. 343, 708–736.
Wang, C., Liu, X., Chen, J.P., Li, K., 2015. Sci. Rep. 5, 16613.
Wang, H., Yin, H., Huang, H., Li, K., Zhou, Y., Waterhouse, G.I.N., Lin, H., Ai, S., 2018a. Biosens. Bioelectron. 108, 89–96.
Wang, Y., Zhou, Y., Xu, L., Han, Z., Yin, H., Ai, S., 2018b. Sens. Actuators B: Chem. 257, 237–244.
Wang, Z., Yan, Z., Wang, F., Cai, J., Guo, L., Su, J., Liu, Y., 2017. Biosens. Bioelectron. 97, 107–114.
Wu, R., Jiang, D., Wang, Y., Wang, X., 2016. Mol. Biotechnol. 58, 450–459.
Yan, Z., Wang, F., Deng, P., Wang, Y., Cai, K., Chen, Y., Wang, Z., Liu, Y., 2018. Biosens. Bioelectron. 109, 132–138.
Yin, H., Zhou, Y., Yang, Z., Guo, Y., Wang, X., Ai, S., Zhang, X., 2015. Sens. Actuators B: Chem. 221, 1–6.
Zhang, Y., Zhou, J., Feng, Q., Chen, X., Hu, Z., 2018. Chemosphere 212, 523–532.
Zhou, Y., Sui, C., Yin, H., Wang, Y., Wang, M., Ai, S., 2018. Microchim. Acta 185, 453.
Zhou, Y., Yin, H., Sui, C., Wang, Y., Ai, S., 2019. Chem. Eng. J. 357, 94–102.